Liu *et al. Energy Mater.* **2025**, *5*, 500059
DOI: 10.20517/energymater.2024.187

Energy Materials

Article

Open Access

Check for updates

Printable high-performance iontronic power source based on osmotic effects

Yanhui Liu[1,2,#], Puguang Peng[1,2,#], Feiyao Yang[1], Zhong Lin Wang[1,3,4,*], Di Wei[1,5,*]

[1]Beijing Institute of Nanoenergy and Nanosystems, Chinese Academy of Sciences, Beijing 101400, China.
[2]School of Nanoscience and Engineering, University of Chinese Academy of Sciences, Beijing 100049, China.
[3]Beijing Key Laboratory of Micro-Nano Energy and Sensor, Center for High-Entropy Energy and Systems, Beijing Institute of Nanoenergy and Nanosystems, Chinese Academy of Sciences, Beijing 101400, China.
[4]Guangzhou Institute of Blue Energy, Knowledge City, Guangzhou 510555, Guangdong, China.
[5]Centre for Photonic Devices and Sensors, University of Cambridge, Cambridge CB3 0FA, UK.
[#]Authors contributed equally.

*__Correspondence to:__ Prof. Zhong Lin Wang and Prof. Di Wei, Beijing Institute of Nanoenergy and Nanosystems, Chinese Academy of Sciences, Yangyan East 1st Road, Yanxi Economic Development Zone, Huairou Dist, Beijing 101400, China. E-mail: zhong.wang@mse.gatech.edu; dw344@cam.ac.uk

How to cite this article: Liu, Y.; Peng, P.; Yang, F.; Wang, Z. L.; Wei, D. Printable high-performance iontronic power source based on osmotic effects. *Energy Mater.* **2025**, *5*, 500059. https://dx.doi.org/10.20517/energymater.2024.187

Received: 24 Sep 2024 **First Decision:** 14 Nov 2024 **Revised:** 29 Nov 2024 **Accepted:** 9 Dec 2024 **Published:** 26 Feb 2025

Academic Editor: Sining Yun **Copy Editor:** Ping Zhang **Production Editor:** Ping Zhang

Abstract

Iontronic power sources have attracted widespread attention in the field of energy harvesting and storage. However, conventional devices only generate an output voltage of ~1.0 V. Herein, we have developed units with an ultra-high voltage of ~2.0 V per unit based on osmotic effects and fine-tuning interfacial redox reactions. These systems are designed to harness the efficient ion dynamics of K^+ within graphene oxide nanofluidic channels and tailor Faradaic processes at the interfaces. Printable, scalable, and optimized through fractal design, these miniaturized units are capable of directly powering commercial electronics, presenting a transformative paradigm for salinity gradient-based power generation. This approach offers a safe, ultra-thin, and portable solution for next-generation energy systems.

Keywords: Printable iontronic power source, osmotic effects, ion dynamics, graphene oxide, nanofluidic channels

INTRODUCTION

Unlike conventional electronics, which rely exclusively on electrons driven by electric fields, iontronics

utilizes multi-type physical and chemical fields to control the ions migration, enabling efficient ion dynamics as charge carriers[1-5]. Precise ion regulation within ionic channels is critical for life-sustaining processes, such as osmotic power generation and neural signal transmission[6,7]. By emulating the structural and functional aspects of these biological ionic channels, researchers have achieved significant advancements in fields such as energy harvesting and storage, ionic logic circuits, and neuromorphic computing[8-12]. The optimization of ion selectivity and permeability is crucial for efficient ion transport and energy conversion[13,14]. Studies have demonstrated that when the diameter of the nanofluidic channel is reduced to less than 100 nm, the electrostatic forces from the electrical double layers (EDLs) of the channel become dominant in the ion transport process[15,16]. These nanofluidic characteristics could facilitate rapid ion transport and significantly enhance ion selectivity at the same time[1,17]. Within the nanoconfined spaces, a series of anomalous ionic behaviors emerge, such as EDL overlap, ionic Coulomb blockade, superionic states, drastic changes in diffusion coefficients, ion correlations, ultra-dense packing of ions, *etc.*[18-22], which provide an opportunity to utilize osmotic effects in nanoconfined iontronics.

To gain deeper insights into ion dynamics at the nanoscale, researchers have utilized nanofluidic materials such as MoS_2, metal-organic frameworks (MOFs) and graphene oxide (GO)/Mxene to construct artificial 0D nanopores, 1D nanotubes, and two-dimensional (2D) nanofluidic channels[23-26]. Owing to their unique structures and surface properties, these nanofluidic channels offer an ideal platform for achieving efficient ion transport. Among these, GO stands out for its abundant 2D nanofluidic channels and negatively charged surface functional groups, which can significantly promote cation transport[27-30]. These channels have been widely applied in various energy harvesting and conversion technologies due to their high ion selectivity and permeability. More importantly, the 2D nanofluidic channels of GO can be fabricated on a large scale using simple drop-casting or printing methods, circumventing the need for complex electron-beam or photolithography techniques. Consequently, a series of iontronic power sources have been developed based on GO films and the osmotic effect[27,29,31,32]. Such solid-state and planar printable iontronic power sources generated a voltage of ~1.0 V, which could be driven purely by humidity in ambient air.

In this study, a solid-state iontronic power source was developed by leveraging osmotic effect within GO nanoconfined spaces and enhancing interfacial redox reaction kinetics through precise regulation, achieving an impressive output voltage of up to ~2.0 V (per unit) at 60% relative humidity (RH). Both experimental results and theoretical calculations reveal that the high performance might arise from the efficient ion dynamics of potassium ions (K^+) within the 2D nanofluidic channels of GO. The electrochemical field, generated by redox reactions between silver (Ag) iodide and aluminum (Al) electrodes at the ionic-electronic interfaces, markedly enhances the output voltage, thereby augmenting the practical applicability of the power source. Furthermore, the entire device can be fabricated on a substrate using printing technology, with its energy capacity augmented by Peano fractal curves. This approach could maximize energy of the iontronic power source in a given area. We demonstrate the potential applications of this iontronic power source in wearable electronics, where even small iontronic units can effectively power commercial electronic devices.

EXPERIMENTAL

Materials

The graphite powder (C, 99.0 wt%) was purchased from Pioneer Nano (XFNANO, INC) Materials Technology Co., Ltd. Acetone (99.5%), ethanol (99.5%), Silver nitrate ($AgNO_3$), phosphoric acid (H_3PO_4, 85.0 wt% in H_2O), potassium permanganate ($KMnO_4$, 99.5%), hydrogen peroxide solution (H_2O_2, 30 wt% in H_2O) concentrated sulfuric acid (H_2SO_4), and Potassium hydroxide (KOH, 88.5% AR) were purchased from Sigma-Aldrich. Deionized (DI) water with a resistivity > 18 MΩ·cm^{-1} was prepared using the Milli-Q Biocel

(ZIQ7000T0C, America) system. Conductive Ag was purchased from Changsung Corporation. Aluminum paste was self-prepared using aluminum powder purchased from Feng Ye Metal Materials.

Fabrication for Ag and Al layer charge collectors

The polyethylene terephthalate (PET) films were ultrasonically cleaned and dried by placing them in acetone, ethanol and DI water, respectively, in sequence. The customized PET films are cut using a computer-controlled commercial CO_2 laser cutting and engraving system. Thus, conductive silver ink and aluminum paste were printed onto a PET film according to a pre-designed pattern using the screen printing method. The distance between the silver and aluminum current collectors is 2 mm. The obtained substrates printed with current collectors were placed at 60 °C for 30 min for drying.

Preparation process for GO powder and GO aqueous solution

GO was prepared by modified Hummer's method using graphite powder as raw material. Initially, 1 g of graphite powder, 2 mL of H_3PO_4, and 21 mL of H_2SO_4 are pre-mixed uniformly under ice bath conditions. Then, 3 g of $KMnO_4$ is slowly added to the pre-mixed solution, allowing it to react thoroughly for 2 h. The pre-oxidized solution was placed in a water bath at 40 °C and stirred thoroughly for 60 min to form a thick paste-like solution. Subsequently, 45 mL of DI water was slowly added to the above solution and heated in a water bath at 95 °C for 15 min. Finally, 150 mL of DI water and 10 mL of H_2O_2 were added to the above solution and the color of the solution changed from dark brown to bright yellow. To wash away soluble salts and unreacted graphite, the reacted GO solution is subjected to multiple centrifugation steps. The collected brownish-yellow clear liquid is the GO dispersion. The supernatant is collected and freeze-dried to obtain GO powder.

Preparation process for GO aqueous solution

An aqueous $AgNO_3$-doped GO solution was formed by adding 1.699 g of $AgNO_3$ and 50 mg of GO lyophilized powder to 10 ml of DI water with vigorous stirring and ultrasonication to homogeneously mix the solution, where GO powder was used to modulate its rheological properties.

Preparation process for reduced graphene oxide aqueous solution

The reduced GO (rGO) solution was formed by mixing 5 $mg{\cdot}mL^{-1}$ of GO solution and 0.1 $mol{\cdot}L^{-1}$ of KOH solution in a 1:2 volume ratio (v/v) with thorough stirring.

Fabrication processes for iontronic power sources

The charge collectors, GO and rGO, obtained through the aforementioned methods are utilized to assemble iontronic power sources. Apply 10 μL of the $AgNO_3$-doped GO solution to one side of the screen-printed silver current collector and 10 μL of rGO to the Al electrode side. After drying, place the device in a constant temperature and humidity chamber for testing.

Measurements and material characterizations

All electrochemical characterizations were performed using a Swiss Metrohm Multi-channel electrochemical workstation (Multi Autolab M204, Netherlands). All electrochemical testing of the devices was performed in a high and low temperature humidity and heat environmental chamber (Voetschtechnik PRO C/340/40/3, China). The ZX21g rotary resistance box was used as an external adjustable load resistor to test the device's voltage and current changes with varying load resistance, thereby determining the device's output power. Dektak XT Stylus three-dimensional (3D) surface profilometer (Bruker Contour GT-K, USA) was used to measure material surface roughness from nm to mm scale. Raman analysis and Raman imaging were performed using a laser confocal microscopy Raman spectroscopy system (Horiba SR-500i-A, UK) equipped with a transmission electron microscopy (TEM) single-frequency laser

(λ = 532 nm, laser power = 40 mW, WITec GmbH, Germany). The device's morphology features were observed using a dual-beam field emission scanning electron microscope (FIB-SEM, Helios NanoLab 600i, USA) with an accelerating voltage of 5 kV and an emission current of 10 μA, and elemental analysis was conducted using energy-dispersive X-ray spectroscopy (EDX). The Zeta potential of the samples was measured using a Zeta potential analyzer (Delsamax Pro, Beckman Coulter). Functional groups and chemical bonds in the samples were analyzed using a Fourier-transform infrared spectrometer (FTIR, VERTEX 80v, Bruker). Optical images of the device were observed using a metallurgical microscope (UMT203i, Chongqing UOP). The crystal structure property profiles of the samples were obtained by an X-ray diffractometer (XRD, Bruker D8 Advance, Germany) with an operating voltage of 40 kV.

Simulation of computational methods

Density functional theory (DFT) calculations are used to investigate the interactions between Li^+, Na^+, K^+, Ca^{2+}, and H_2O. The wave function expansion was truncated at 500 eV, with an energy convergence criterion set to 10^{-6} eV and the force convergence criterion is set to 0.01 eV·Å to ensure high precision in the calculations. The Perdew-Burke-Ernzerhof (PBE) functional within the framework of the generalized gradient approximation (GGA) was employed to handle the exchange and correlation terms.

RESULTS AND DISCUSSION

Unlike the passive diffusion of H_2O and gases across cellular membranes, the transport of inorganic salt ions (e.g., Na^+, K^+, and Ca^{2+}) within biological systems is mediated by specific carrier proteins. These proteins facilitate the entry and exit of ions from cells [Figure 1A], thereby generating action potentials. The distinct ion channels underpin diverse electrical signaling mechanisms and high-speed communication across membranes. Artificial nanochannels have been constructed to study ion transport behavior under nanofluidic spaces. Ion transport within 2D nanofluidic channels is pivotal to the research and performance of iontronic power sources. It has been reported that the low ion charge and weakly bound hydration shells of K^+ can promote the entry of hydrated ions into nanochannels, leading to higher conductivity[32-34]. DFT calculations were performed to determine the desolvation energy barriers of various ions in the presence of a single water molecule [Supplementary Figure 1]. The simulation results indicated that K^+ exhibited the lowest binding energy with water molecules, leading to its selection as the cation for diffusion within the GO 2D nanofluidic channels. The efficiency of ion transport is largely determined by the desolvation energy barriers of ions within their hydration shells and surface charge density of nanofluidic channels[35,36]. Lower binding energies of target ions translate to reduced activation energy for entrance, thereby enhancing the overall performance of the iontronic power source.

The overall structure of the iontronic power source is illustrated in Figure 1B. The schematic diagram of the iontronic power source and the SEM image of the GO/rGO junction are shown in Supplementary Figure 2. The device was fabricated using screen-printing technology, where silver and aluminum electrodes were first printed on the surface of a PET film, with a 2 mm gap between the electrodes. To introduce the electrode interface reaction, 1 M $AgNO_3$ was coated and dried on the Ag electrode surface. To establish an asymmetric ion concentration gradient, two distinct GO-based inks were prepared. GO synthesized via the modified Hummers' method displays a characteristic layered structure [Supplementary Figure 3]. Its selection as the 2D nanofluidic material is attributed to this layered architecture, which is rich in oxygen-containing functional groups (-COOH, -OH, -C=O, and -C-O, Supplementary Figure 4) and a high zeta potential (-40.39±3.76 mV, Supplementary Figure 5). Its high negative surface charge allows for the rapid unidirectional transport of cations, especially in its horizontal direction, resulting in high permeability. GO ink (5 mg·mL^{-1}) was sequentially printed onto the Ag current collector following the printing of $AgNO_3$, establishing 2D nanofluidic channels for the iontronic power source. To introduce a

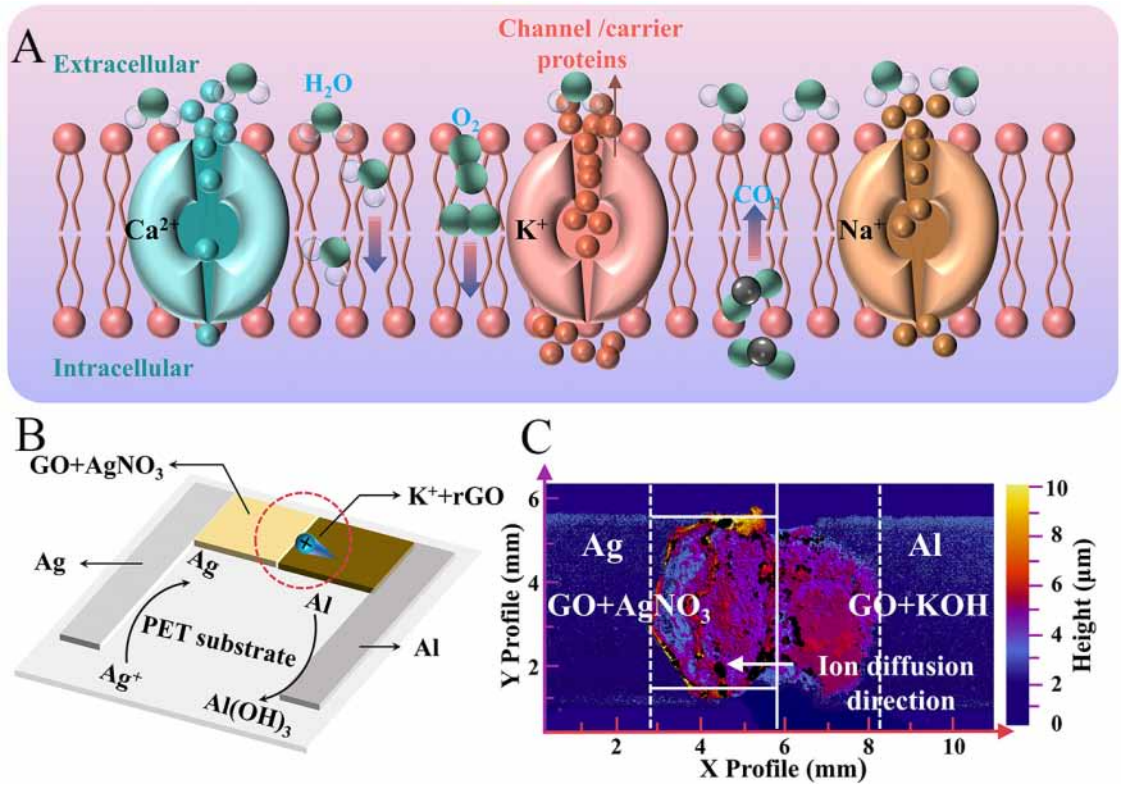

Figure 1. (A) Schematic diagram of the transportation of substances in the cells of an organism. H_2O and O_2 move in and out of cells through a process of free diffusion; (B) Schematic diagram of the 3D structure of the iontronics; (C) 3D surface profile of the iontronics. 3D: Three-dimensional.

high ion gradient, KOH was added to the GO ink to produce rGO. Notably, the reduction of GO with a controlled concentration of KOH does not compromise its solubility. It has been reported that GO undergoes a series of deoxygenation reactions under alkaline conditions to form a soluble solution, and the potassium salts do not crystallize or separate from the GO after drying[32]. Importantly, while the color of the rGO solution transitions from light brown to dark brown, the reaction at room temperature only partially removes the functional groups of GO, preserving its hydrophilic properties[37,38]. As a result, 1M rGO was printed on an Al anode to be used as a K^+ cation reservoir. The rGO is also connected to the GO to form a heterojunction for ion transport. Therefore, K^+ ions can diffuse from the rGO side through the 2D nanofluidic channels to the GO side to release the osmotic power. In addition, the OH^- in rGO can also react with an Al electrode to form a redox electric pair with the Ag electrode. The introduction of interfacial redox reactions leads to the built-in internal electrochemical field, which promotes the directional diffusion of ions, increasing the current output of the iontronic power source. Such an all-printable fabrication process makes our iontronic power source ultra-thin and flexible. The 3D surface profilometer [Figure 1C] analysis of the iontronic power source reveals that the total thickness of the device is about 10 μm, with the GO layer thickness of approximately 5 μm as shown in Supplementary Figure 6. The effective ion diffusion area is 1.86×10^{-8} m^2, as calculated in Supplementary Note 1; large osmotic power can be realized in a small nanofluidic space.

Figure 2A shows the high voltage output of our iontronic power source. Under the conditions of 60% RH and 25 °C, the device could generate an open-circuit voltage of ~2 V. This voltage output can also keep at ~1.75 V even after 25 h, with a voltage retention rate near 90%. Figure 2B presents the current-voltage (I-V)

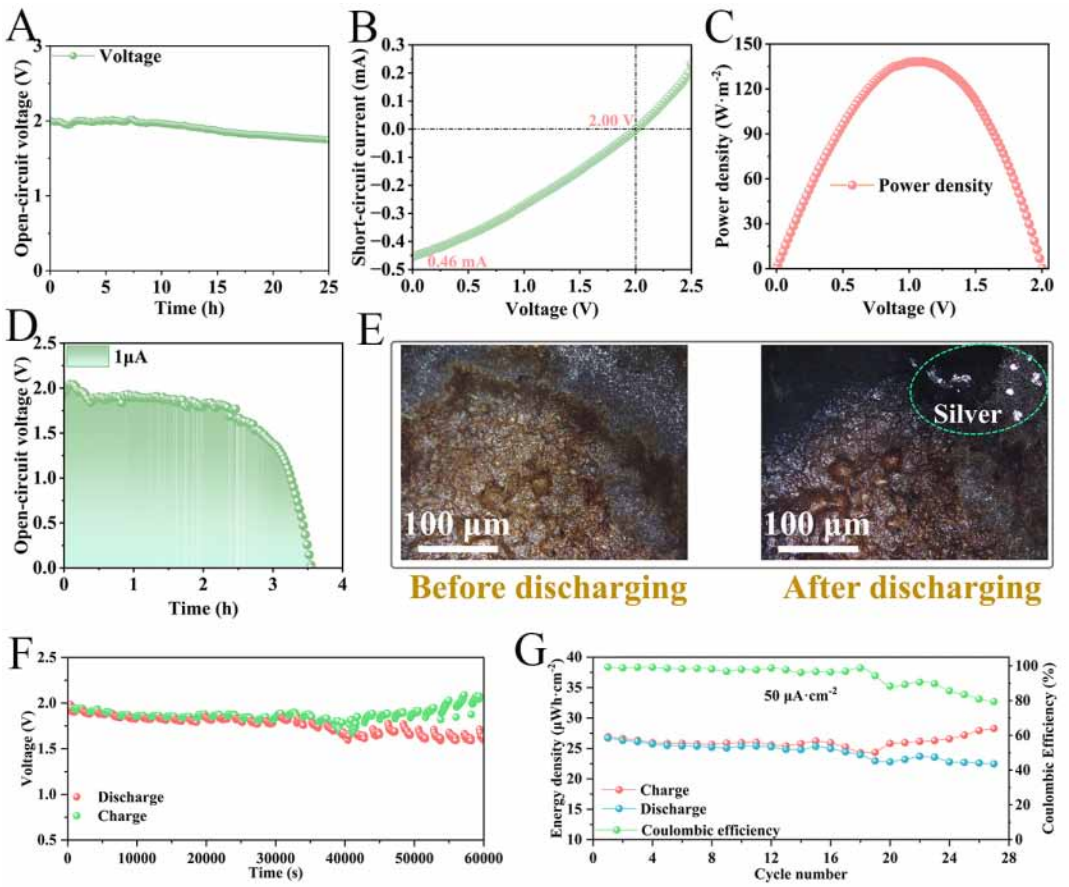

Figure 2. (A) V_{OC} of the iontronic power source at 60% relative humidity; (B) The I-V characteristic curve of the Ag/$AgNO_3$-GO/KOH-rGO/Al power system; (C) The areal power density output of the iontronic power source without an external load resistance; (D) The discharge curve of the iontronic power source at a constant current of 1 μA; (E) Optical images of the GO/$AgNO_3$ at the cathode of the power source. The photos were taken before discharge (left) and after discharge (right); (F) The constant current discharge curve of the iontronic power source at 1 μA; (G) The charge-discharge cycle stability and coulombic efficiency of the iontronic power source system at 1 μA. GO: Graphene oxide; rGO: reduced GO; Ag: silver; Al: aluminum.

curve of the iontronic power source, measured using linear sweep voltammetry under a voltage range of 0-2.5 V and a scan rate of 100 $mV \cdot s^{-1}$. The iontronic power source can achieve an areal short-circuit current density of up to $235 \cdot A \cdot m^{-2}$, and the open circuit voltage of I-V test is consistent with the previous results in Figure 2A. The current enhancement in iontronic power sources is likely due to ion migration driven by the built-in electric field and the Coulomb drag effect[39,40]. The power density of the iontronic power source was calculated from the I-V curve to be 138.1 $W \cdot m^{-2}$ [Figure 2C]. Such a high power density allows the iontronics power sources to be discharged at a constant high current of 1 μA and achieve a volumetric energy density of 604 Wh m^{-3}, as shown in Figure 2D. Compared to the output of traditional ionotronic power sources, such as moist-electric generators (MEGs) and water evaporation-induced electric generators (WEGs), the voltage and current output of the iontronic power source in the present work exhibit a significant competitive advantage [Supplementary Table 1].

The high performance may come from the fine-tuned reversible redox reactions in the iontronic power source, which facilitates the efficient cation transport within the 2D nanofluidic channels of GO between the electrode potential differences. In detail, at the cathode, the reduction reaction $Ag^+ + e^- \rightleftharpoons Ag$ takes place, while at the anode, the oxidation reaction $Al + 3OH^- - 3e^- \rightleftharpoons Al(OH)_3$ occurs. The high voltage of up to ~2 V

has already exceeded our previous work based on Ag/Ag^+ redox couple due to the optimized electrode redox, which aligns closely with the predictions of the Nernst equation as discussed in Supplementary Note 2. Metallographic microscopy confirms the occurrence of the redox reactions. As illustrated in Figure 2E, the original interface on the GO side is populated with white $AgNO_3$ salt powders, while silver-white silver metal particles precipitate at the interface following discharge. Meanwhile, a white colloidal state was also observed on the rGO (anode) side as shown in Supplementary Figure 7, which is likely $Al(OH)_3$. The ion diffusion in GO nanofluidic channels can be directly observed by XRD as shown in Supplementary Figure 8. The interlayer spacing of the GO sheets in the iontronic power source was 8.60 Å before discharge, and the space increased to 8.75 Å after prolonged discharge, indicating that the ions are embedded in GO. Elemental analyses further substantiate the diffusion of K^+ ions within the 2D nanofluidic channels of GO after discharge [Supplementary Figures 9 and 10, Supplementary Tables 2 and 3]. This iontronic power source is also rechargeable due to the reversible redox reaction at the interface. The charge-discharge curve of the iontronic power source at a constant areal current of 1 μA is shown in Figure 2F. After 60,000 s of constant current charging and discharging cycles, the power source continues to exhibit robust cycle stability and high coulombic efficiency [Figure 2G]. High cyclic stability originates from reversible K^+ diffusion and reversible electrode reactions. This advancement enables iontronic power sources to overcome the inherent limitations of low output current and power in osmotic power devices, making significant progress toward achieving portability and printability for these devices.

The iontronic power source maintains a high-power output when connected to an external load, making it more capable of driving microelectronic devices in everyday life. The voltage and current output of the power source across various load resistances are shown in Figure 3A. The insert illustrates the connection configuration of the test circuit. As the external load resistance increases, the voltage rises, while the current shows a decreasing trend. The optimal output power of the iontronic power source is 74.1 $W \cdot m^{-2}$ when the external load resistance is 7 kΩ [Figure 3B]. The detailed calculation method can be found in Supplementary Note 3. The voltage output for 1, 2, and 3 series-connected units are 1.97 V, 3.92 V, and 6.10 V, respectively [Figure 3C]. The voltage output of the series power supply increases linearly with the number of devices, indicating the devices have excellent scalability. Iontronic power sources can be printed using GO and rGO inks with good rheological properties, as shown in Figure 3D. The relationship between the viscosity of GO ink and shear rate is shown in Supplementary Figure 11, indicating that the GO ink exhibits ideal shear-thinning behavior, which enables continuous inkjet printing and rapid curing. An iontronic power source featuring Peano curves has been fabricated, demonstrating the highest areal power density output in a given area. The Peano curve mask was made by laser cutting following the screen printing of the predefined charge collector pattern, after which GO and rGO inks are precisely printed, finalizing the patterned iontronic power source.

By connecting multiple iontronic power sources in series, they can generate sufficient voltage to power commonly used small electronics. As shown in Figure 3E and Supplementary Video 1, integrating three iontronic power sources can power an electronic watch. Three integrated devices can power a watch for over 6 h at 25 °C and 45% RH [Supplementary Figure 12]. In addition, the integrated power source is capable of powering commercial calculators [Figure 3F and Supplementary Video 2] and light-emitting diode (LED) lights [Figure 3G and Supplementary Video 3], further demonstrating the potential of ionic electronic power sources in practical applications as efficient power devices. Iontronic power sources can not only directly power electronics but also store the generated electricity in capacitors for later use. A single iontronic power source can charge an aluminum electrolytic capacitor to 2 V within 20 s, as demonstrated in Supplementary Figure 13. This lightweight, ultra-thin, safe, and printable ionic electronic power source provides a stable energy supply for wearable electronic devices.

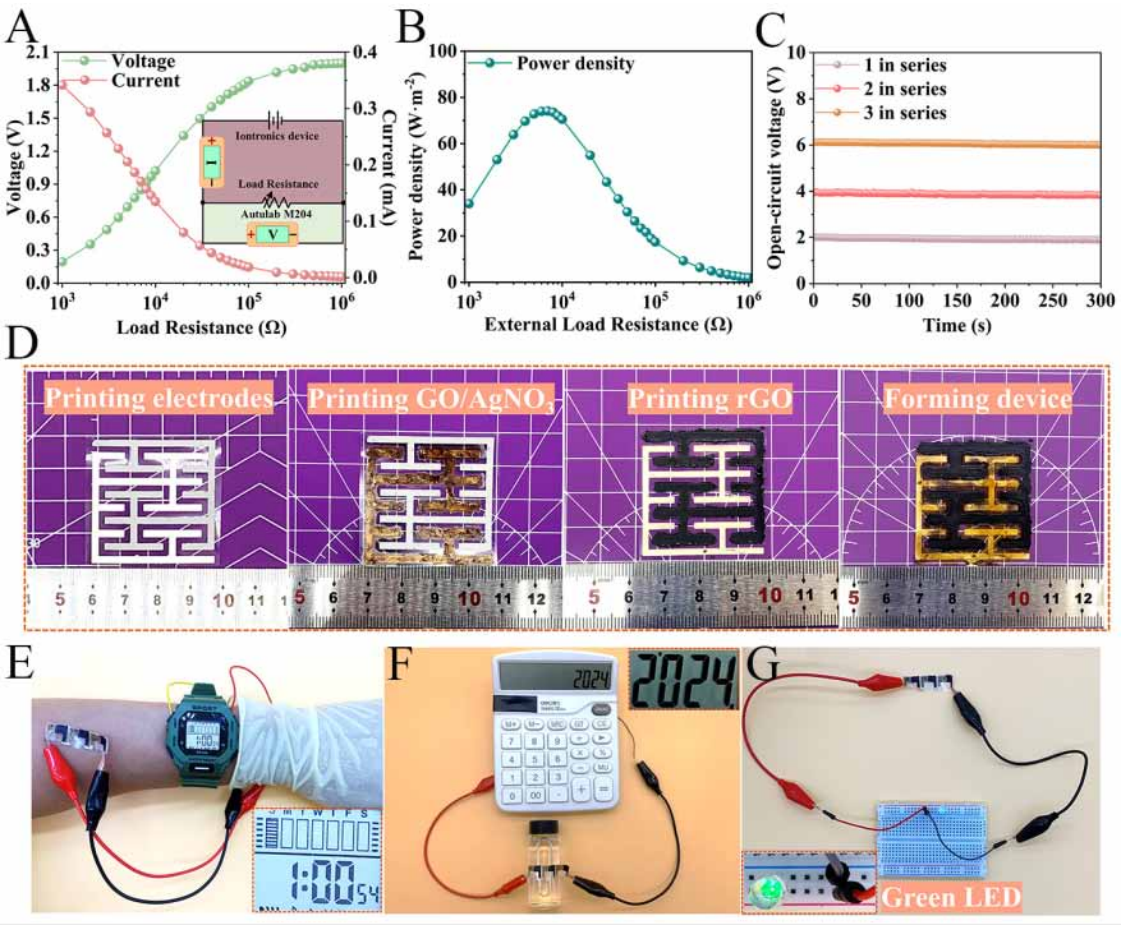

Figure 3. (A) The voltage and current output of the iontronic power source under different external load resistances; (B) Areal Power density output of the power source under different external load resistances; (C) Output voltage curves for different numbers of devices in series; (D) Printing of patterned iontronic power source; (E) The iontronic power supply is connected in series to drive the electronic watch; (F) The power supply is connected in series to drive the calculator; (G) The power source is connected in series to drive the LEDs. LED: Light-emitting diode.

CONCLUSIONS

In summary, an all-solid-state iontronic power source system has been proposed, demonstrating superiority over conventional salinity gradient energy conversion devices. The system harnesses the synergistic effects of anomalous ionic transport in 2D nanofluidic channels and the tailored interfacial Faraday reactions. DFT calculations confirmed efficient ion dynamics of K^+ within the 2D nanofluidic channels of GO. With the assistance of the $Al/Al(OH)_3$ and Ag/Ag^+ redox pairs, the iontronic power source can achieve a voltage output of up to 2 V, and the built-in internal electrochemical field accelerates the directed diffusion of K^+ ions. The solid-state iontronic power source can achieve an optimal output power density of 74.1 W m^{-2} when the external load resistance is 7 kΩ. The iontronic power source employs a novel approach that utilizes enhanced ion dynamics while customizing interfacial redox reactions to significantly enhance energy conversion via osmotic effects. This methodology not only offers valuable insights but also establishes new paradigms for osmotic devices, advancing the efficient harnessing of salinity gradient power generation.

DECLARATIONS

Authors' contributions

Made substantial contributions to conception and design of the study and performed data analysis and interpretation: Liu, Y.; Peng, P.
Wrote the first version of the manuscript: Liu, Y.
Provided technical and material support: Yang, F.
Supervision, writing - review and editing: Wang, Z. L.; Wei, D.
All authors revised the manuscript.

Availability of data and materials

The data are available upon request from the authors.

Financial support and sponsorship

This work was supported by the National Natural Science Foundation (grant number 22479016).

Conflict of interest

All authors declared that there are no conflicts of interest.

Ethical approval and consent to participate

Not applicable.

Consent for publication

Not applicable.

REFERENCES

1. Peng, P.; Qian, H.; Liu, J.; Wang, Z.; Wei, D. Peng P, Qian H, Liu J, Wang Z, Wei D. Bioinspired ionic control for energy and information flow. *Int. J. Smart. Nano. Mater.* **2024**, *15*, 198-221. DOI
2. Graf, M.; Lihter, M.; Unuchek, D.; et al. Light-enhanced blue energy generation using MoS_2 nanopores. *Joule* **2019**, *3*, 1549-64. DOI
3. Tsutsui, M.; Hsu, W. L.; Garoli, D.; et al. Gate-all-around nanopore osmotic power generators. *ACS. Nano.* **2024**, *18*, 15046-54. DOI
4. Liu, P.; Kong, X. Y.; Jiang, L.; Wen, L. Ion transport in nanofluidics under external fields. *Chem. Soc. Rev.* **2024**, *53*, 2972-3001. DOI PubMed
5. Liu, P.; Gao, X.; Zhang, L.; et al. Osmotic-enhanced-photoelectrochemical hydrogen production based on nanofluidics. *CCS. Chem.* **2023**, *5*, 2012-22. DOI
6. Esfandiar, A.; Radha, B.; Wang, F. C.; et al. Size effect in ion transport through angstrom-scale slits. *Science* **2017**, *358*, 511-3. DOI
7. Zhang, Z.; Wen, L.; Jiang, L. Nanofluidics for osmotic energy conversion. *Nat. Rev. Mater.* **2021**, *6*, 622-39. DOI
8. Xin, W.; Zhang, Z.; Huang, X.; et al. High-performance silk-based hybrid membranes employed for osmotic energy conversion. *Nat. Commun.* **2019**, *10*, 3876. DOI PubMed PMC
9. Mei, T.; Liu, W.; Xu, G.; et al. Ionic transistors. *ACS. Nano.* **2024**, *18*, 4624-50. DOI
10. Kim, S.; Choi, S.; Lee, H. G.; et al. Neuromorphic van der Waals crystals for substantial energy generation. *Nat. Commun.* **2021**, *12*, 47. DOI PubMed PMC
11. Xin, W.; Fu, J.; Qian, Y.; et al. Biomimetic KcsA channels with ultra-selective K^+ transport for monovalent ion sieving. *Nat. Commun.* **2022**, *13*, 1701. DOI PubMed PMC
12. Tang, J.; Wang, Y.; Yang, H.; et al. All-natural 2D nanofluidics as highly-efficient osmotic energy generators. *Nat. Commun.* **2024**, *15*, 3649. DOI PubMed PMC
13. Li, C.; Wen, L.; Sui, X.; Cheng, Y.; Gao, L.; Jiang, L. Large-scale, robust mushroom-shaped nanochannel array membrane for ultrahigh osmotic energy conversion. *Sci. Adv.* **2021**, *7*, eabg2183. DOI PubMed PMC
14. Shen, J.; Liu, G.; Han, Y.; Jin, W. Artificial channels for confined mass transport at the sub-nanometre scale. *Nat. Rev. Mater.* **2021**, *6*, 294-312. DOI
15. Zhong, J.; Alibakhshi, M. A.; Xie, Q.; et al. Exploring anomalous fluid behavior at the nanoscale: direct visualization and quantification via nanofluidic devices. *Acc. Chem. Res.* **2020**, *53*, 347-57. DOI

16. Forse, A.; Griffin, J.; Merlet, C.; et al. Direct observation of ion dynamics in supercapacitor electrodes using in situ diffusion NMR spectroscopy. *Nat. Energy.* **2017**, *2*, 2016216. DOI
17. Qian, H.; Wei, D.; Wang, Z. Bionic iontronics based on nano-confined structures. *Nano. Res.* **2023**, *16*, 11718-30. DOI
18. Xue, Y.; Xia, Y.; Yang, S.; et al. Atomic-scale ion transistor with ultrahigh diffusivity. *Science* **2021**, *372*, 501-3. DOI
19. Wang, M.; Hou, Y.; Yu, L.; Hou, X. Anomalies of ionic/molecular transport in nano and sub-nano confinement. *Nano. Lett.* **2020**, *20*, 6937-46. DOI
20. Daiguji, H. Ion transport in nanofluidic channels. *Chem. Soc. Rev.* **2010**, *39*, 901-11. DOI PubMed
21. Robin, P.; Bocquet, L. Nanofluidics at the crossroads. *J. Chem. Phys.* **2023**, *158*, 160901. DOI PubMed
22. Zhan, H.; Xiong, Z.; Cheng, C.; Liang, Q.; Liu, J. Z.; Li, D. Solvation-involved nanoionics: new opportunities from 2D nanomaterial laminar membranes. *Adv. Mater.* **2020**, *32*, e1904562. DOI
23. Zhu, C.; Liu, P.; Niu, B.; et al. Metallic two-dimensional MoS_2 composites as high-performance osmotic energy conversion membranes. *J. Am. Chem. Soc.* **2021**, *143*, 1932-40. DOI
24. Yang, L.; Cao, L. N.; Li, S.; et al. MOFs/MXene nano-hierarchical porous structures for efficient ion dynamics. *Nano. Energy.* **2024**, *129*, 110076. DOI
25. Yang, L.; Li, S.; Qian, H.; Wang, Z.; Wang, Z. L.; Wei, D. Osmotic power generation based on nanoconfined materials. *MRS. Energy. Sustain.* **2024**, *11*, 193-218. DOI
26. Qian, H.; Peng, P.; Fan, H.; et al. Horizontal transport in $Ti_3C_2T_x$ MXene for highly efficient osmotic energy conversion from saline-alkali environments. *Angew. Chem. Int. Ed.* **2024**, *63*, e202414984. DOI
27. Yang, F.; Peng, P.; Yan, Z.; et al. Vertical iontronic energy storage based on osmotic effects and electrode redox reactions. *Nat. Energy.* **2024**, *9*, 263-71. DOI
28. Peng, P.; Yang, F.; Wang, Z.; Wei, D. Integratable paper-based iontronic power source for all-in-one disposable electronics. *Adv. Energy. Mater.* **2023**, *13*, 2302360. DOI
29. Wei, D.; Yang, F.; Jiang, Z.; Wang, Z. Flexible iontronics based on 2D nanofluidic material. *Nat. Commun.* **2022**, *13*, 4965. DOI PubMed PMC
30. Peng, P.; Yang, F.; Li, X.; Li, S.; Wang, Z.; Wei, D. High-power iontronics enabled by nanoconfined ion dynamics. *Cell. Rep. Phys. Sci.* **2024**, *5*, 101824. DOI
31. Wei, D. Writable electrochemical energy source based on graphene oxide. *Sci. Rep.* **2015**, *5*, 15173. DOI PubMed PMC
32. Yang, L.; Yang, F.; Liu, X.; et al. A moisture-enabled fully printable power source inspired by electric eels. *Proc. Natl. Acad. Sci. U. S. A.* **2021**, 118. DOI PubMed PMC
33. Abraham, J.; Vasu, K. S.; Williams, C. D.; et al. Tunable sieving of ions using graphene oxide membranes. *Nat. Nanotechnol.* **2017**, *12*, 546-50. DOI
34. Nightingale, E. R. Phenomenological theory of ion solvation. Effective radii of hydrated ions. *J. Phys. Chem.* **1959**, *63*, 1381-7. DOI
35. Huang, A.; Ma, Z.; Kumar, P.; et al. Low-temperature and fast-charging lithium metal batteries enabled by solvent-solvent interaction mediated electrolyte. *Nano. Lett.2024*, 7499-507. DOI
36. Xiong, M.; Athreya, N.; Chakraborty, R.; Leburton, J. P. Ion trapping and thermionic emission across sub-nm pores. *Nano. Lett.* **2023**, *23*, 11719-26. DOI PubMed
37. Fan, X.; Peng, W.; Li, Y.; et al. Deoxygenation of exfoliated graphite oxide under alkaline conditions: a green route to graphene preparation. *Adv. Mater.* **2008**, *20*, 4490-3. DOI
38. Pei, S.; Cheng, H. The reduction of graphene oxide. *Carbon* **2012**, *50*, 3210-28. DOI
39. Xiong, M.; Song, K.; Leburton, J. Ionic coulomb drag in nanofluidic semiconductor channels for energy harvest. *Nano. Energy.* **2023**, *117*, 108860. DOI
40. Jiang, Y.; Liu, W.; Wang, T.; et al. A nanofluidic chemoelectrical generator with enhanced energy harvesting by ion-electron coulomb drag. *Nat. Commun.* **2024**, *15*, 8582. DOI PubMed PMC